*35th EPS Conference on Plasma Phys. Hersonissos, 9 - 13 June 2008 ECA Vol.**32D**, P-5.109 (2008)*

Fast Electron Propagation In High Density Plasmas Created By Shock Wave Compression

J. J. Santos[1], D. Batani[2], P. McKenna[3], S. D. Baton[4], F. Dorchies[1], A. Dubrouil[1], C. Fourment[1], S. Hulin[1], Ph. Nicolaï[1], M. Veltcheva[2], P. Carpeggiani[2], M. Quinn[3], E. Brambrink[4], M. Koenig[4], M. Rabec Le Glohaec[4], Ch. Spindloe[5], M. Tolley[5]

[1] *CELIA, Université Bordeaux 1-CNRS-CEA, Talence, France*

[2] *Dipartimento di Fisica "G. Occhialini", Univ. degli Studi di Milano-Bicocca, Milan, Italy*

[3] *SUPA, Dpt. Physics, University of Strathclyde, Glasgow, UK*

[4] *LULI, Ecole Polytechnique - CNRS - CEA, Palaiseau, France*

[5] *Rutherford Appleton Laboratory, Chilton, Didcot, UK*

Till now almost all the experimental results on fast electron generation and transport have been obtained in solid targets. It is clear instead that the fast ignitor approach to inertial fusion concerns the propagation of a fast electron beam in a dense hot plasma surrounding the nuclear fuel in the pellet. Here we present preliminary results from a recent experiment on fast electrons propagation and energy deposition in high density plasmas created by shock wave compression.

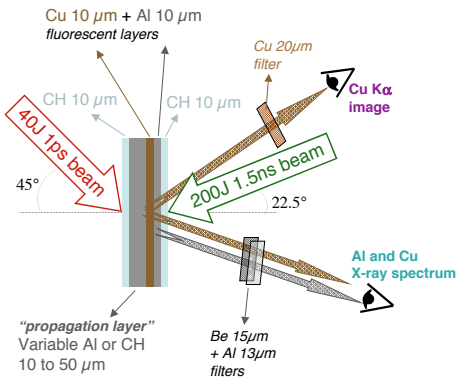

Figure 1: In-principle scheme of the experimental set-up and of the used targets.

The results were obtained at the PICO 2000 laser system at LULI, coupling a 200 J, 1.5 ns, $2\omega_0$ compression beam with a counter-propagating 40 J, 1 ps high-intensity beam. Focusing the ps beam to 10-13 μm diameter spots, we got intensities on target of 3-5 10^{19} Wcm^{-2} capable to generate intense currents of fast electrons through the indepth regions of the target, shock-compressed at 3-4 times the initial solid density. In reality, due to technical constraints in the interaction chamber, the two beams were not exactly counter-propagating, the ns laser beam being focused at 45° on the target *front* side, while the ps beam was focused at 22.5° degrees on the target *rear* side. This does not imply any change in the basic scheme because both the generated shock and the fast electron beam are travelling normally to the target. The scheme of the experiment is shown in Fig. 1.

The diagnostic system was based on incorporating at the rear of the targets a fluorescent bi-layer made of 10 μm Cu and 10 μm Al. The Kα signal from the Cu layer was recorded through a spherical Bragg crystal imaging the X-ray source [1] onto image plates. This imaging diag-

nostic allowed to get 2D images with a 10.8 magnification of the spatial distribution of fast electrons as they cross the Cu tracer (producing ionization followed by Kα emission). This allowed to reconstruct the beam geometry and divergence. The Kα emission from the Al layer was recorded in the 1^{st} diffraction order by a conical crystal X-ray spectrometer [2]. Its spectral resolution of 1.7 eV would allow to measure both the Kα from cold Al atoms and the shifted Kα emission from Al ions. Since the degree of ionisation in the Al layer is a function of temperature, in principle such a diagnostic allows to infer the background temperature in the tracer by measuring the ratio between cold and *hot* Kα lines [3]. The spectrometer also measured the Cu Kα emission in the 5th diffraction order. Both diagnostics allowed measuring the propagation range of fast electrons in the material by plotting the Kα signal vs. target thickness obtained on different shots.

The thickness to be changed was the *propagation layer* (as shown in Fig. 1). We used both *conducting* targets (Al propagation layer) and *insulating* target (plastic layer) in order to compare different materials, which have shown different propagation characteristics in previous works [4, 5], and to see if they behave in a similarly way under shock compression. For each kind of target, the results are compared to the cold case (no compression beam).

In the case of Al layer, the Cu layer also filtered the X-ray emission from the propagation layer, so that only the Al X-rays emitted from the Al tracer layer could reach the spectrometer. Two additional plastic layers, each 10 μm, were added on both sides. On the ns side this served to reduce preheating which could arise from the direct interaction of the ns beam with Al. The presence of plastic on the ps beam was due to the fact that in all cases we wanted the same fast electron source; therefore we chose to have the laser always interacting with a plastic layer. At the same time, plastic reduced any X-ray preheating, which could arise due to the laser prepulse. For the same reason (i.e. maintaining the same fast electron source in all cases), when the ns beam was fired, the ps beam was timed so to be fired before shock breakout (actually leaving the last 10 μm of plastic uncompressed). For different targets, the breakout times were measured by a time-resolved imaging of the *front* side using a streak camera. Finally a very thin Al layer was added onto plastics in order to avoid laser shine-through. These measurements were reproduced by 1D MULTI hydrodynamic simulations.

To correctly understand the X-ray results and to properly model the fast electron generation and transport through the targets, we need to know their exact state (density and temperature profiles) when the ps beam interacts. For that, we must also consider the effects of the ps beam ASE pedestal. Fast diode measurements shown a $2\,10^{-3}$ energy contrast. The pedestal corresponds to a ramp whose FWHM duration of 1.1 ns has been precisely characterized by Wol-

laston interferometry of the pre-plasma formed on the *front* side of the target. A $\approx 100\,\mu$m pre-plasma is measured 250 ± 45 ps before the intense part of the pulse arrival.

Whereas the ns beam induced shocks are reproduced by 1D hydrodynamics, the ps beam small spot size implies a 2D hydrodynamical behavior. We used the 2D hydrodynamic code CHIC to account for both ns beam and ASE-pedestal perturbations. This pedestal produces non negligible effects on the propagation and fluorescent layers, as can be seen in figure 2 for a $10\,\mu$m Al-propagation layer target at time $t_0 + 2.2$ ns, the chosen moment for the UHI interaction (ns-shock breakout had been measured to hapen at $t_0 + 2.6$ ns). There we compare the density profiles for ps and ns+ps interactions. We can clearly identify the ASE-induced shocks and also realize that against our predictions, in the case of the ns+ps interaction, because of the *front* CH layer ablation by the ASE, the target has already expanded due to the ns-shock breakout. This situation can affect the interpretation of the X-ray results (presented further below), as the *front* side density profile (scale gradient and critical density position) are not the same for the two situations, thus probably neither the generated fast electron populations.

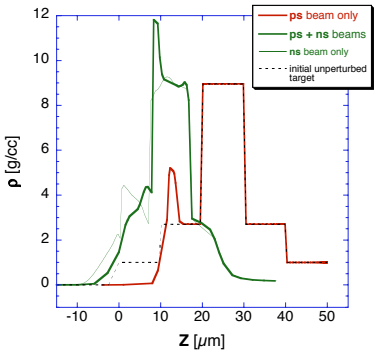

Figure 2: CHIC hydrodynamic calculation: Density profiles for a $10\,\mu$m Al propagation layer target at the intense ps pulse arrival moment.

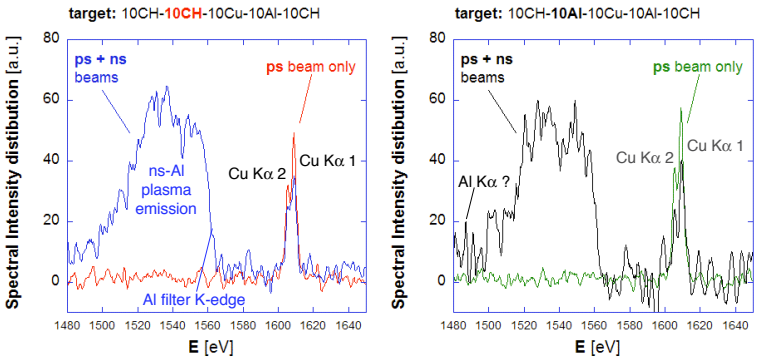

Figure 3: Typical X-ray spectra: solid vs. shock compressed targets for dielectric (left) and conductor (right) propagation layers.

Figure 3 shows typical X-ray spectra, for dielectric (on the left) and conductor $10\,\mu$m propagation layer targets. On each panel we compare the solid (ps beam only) and compressed (ns+ps beams) target cases. For the solid case, we could only detect the Cu Kα lines. On the compressed case they were initially masked by the ~ 500 eV ns-Al plasma He-α emission, which we could elimate by using a supplementar $13\,\mu$m Al filter on the spectrometer. The Al

Kα lines, which we believe to identify on the Al-ns+ps spectrum were almost never detected in this experiment, which invalidates the possibility of measuring the target rear side temperature upon the fast electrons energy deposition.

The Cu Kα spectral lines integrated emissions are compiled in Fig. 4-a) against the propagation layer thickness. We see the signal yields are lower for compressed targets for both Al and CH propagation layers. Without compression, signals are stronger for Al than for CH targets. With compression, signal yields for Al and for CH targets are comparable. These observations are confirmed by the 2D images Cu Kα emission yields. From Fig. 4-b), showing the Cu Kα radius evolution, we see that the fast electron jet divergence is slightly higher in non compressed targets.

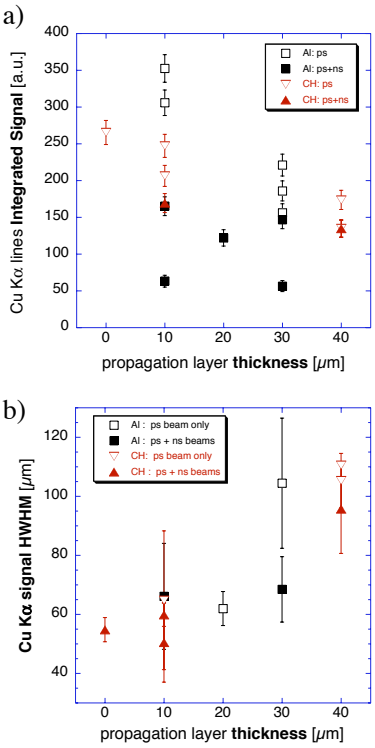

Figure 4: **a)** Cu Kα spectral lines integrated emission and **b)** Cu Kα spot radius (HWHM) as a function of the propagation layer thickness.

If directly correlated to the Cu K yields, we can preliminarly conclude that the fast electron transport is less efficient in compressed matter than in solid density matter. In solid matter, the fast electron transport is more inhibited in CH layers (insulator) due to electric field effects. The fast electron penetration range is equivalent for compressed CH and Al, as both layers are partially ionised and behave like a conducting plasma. Therefore, the collisional stopping power should not be a determinant parameter.

These physical hypothesis still need to be checked by careful modelling and simulations accounting for both hydrodynamics and fast electron induced heating. For each target layer, we must consider density and temperature-depending properties: the collisional stopping power (bound and free electrons + plasmons), the Cu K shell ionization cross section, the electrical conductivity, the electric field transport inhibition and the role of magnetic field.

References

[1] R. B. Stephens *et al.* , Physical Review E, **69**, 066414 (2004)

[2] E. Martinolli *et al.* , Review of Scientific Instruments, **75**, 2024 (2004)

[3] E. Martinolli *et al.* , Physical Review E, **73**, 046402 (2006)

[4] F. Pisani *et al.* , Physical Review E, **62**, R5927 (2000)

[5] M. Manclossi *et al.* , Physical Review Letters, **96**, 125002 (2006)